Synthesis of core-shell magnetic nanoparticles containing ultra-small domains of silicalite-1

Diogenes Honorato Piva, Roger Honorato Piva, Sajjad Ghojavand, Alain Pautrat, Maxime Debost, Ernesto A. Urquieta-González, Svetlana Mintova

Synthesis of core-shell magnetic nanoparticles containing ultra-small domains of silicalite-1

Diógenes Honorato Piva, Roger Honorato Piva, Sajjad Ghojavand, Alain Pautrat, Maxime Debost, Ernesto A. Urquieta-González, Svetlana Mintova**

D.H. Piva, S. Ghojavand, M. Debost, S. Mintova
Laboratoire Catalyse et Spectrochimie
ENSICAEN, Université de Caen
Caen, 14050, France
E-mail: diogenes.piva@ensicaen.fr, svetlana.mintova@ensicaen.fr

R. H. Piva
Science and Technology Center for Energy and Sustainability,
Federal University of Recôncavo of Bahia
Feira de Santana, 44042-280, Brazil

D. H. Piva, E. A. Urquieta-González
Research Center on Advanced Materials and Energy
Federal University of São Carlos
São Carlos, 13565-905, Brazil

M. Debost, A. Pautrat
Laboratoire CRISMAT
CNRS UMR 6508, ENSICAEN
Caen Cedex 4, F-14050 France

Keywords: crystallization, zeolite, core-shell nanostructure, adsorption, magnetic properties

Synthesis of core–shell nanostructures with magnetic core and zeolitic shell is an ongoing challenge. Herein, we present a strategy for preparation of γ-Fe_2O_3@mesoporous silica ($mSiO_2$) core-shell nanoparticles containing ultra-small domains of silicalite-1 in the shell (γ-Fe_2O_3@$mSiO_2$/Silicalite-1). The strategy consists in a solid-state reorganization of the precursor amorphous $mSiO_2$ shell into silicalite-1 using a tetrapropylammonium hydroxide (TPAOH) as an organic structure-directing agent (OSDA) under mild hydrothermal (HT)

conditions. The formation of sililicalite-1 crystalline domains has been investigated through the detailed characterization of products obtained at different times of HT treatment by XRD, Raman spectroscopy, FTIR, SEM with EDS, TEM and nitrogen physisorption. By careful tuning the time of HT treatment, the γ-Fe_2O_3@mSiO_2/Silicalite-1 nanostructures are prepared. Benefitting from the unique mesopores/microporous structure formed, the γ-Fe_2O_3@mSiO_2/Silicalite-1 core-shell nanostructure shows superior adsorption capacity to remove aniline from aqueous solutions than the γ-Fe_2O_3@mSiO_2. Moreover, the γ-Fe_2O_3@mSiO_2/Silicalite-1 nanostructure is easily separated from aqueous solutions using magnetic separation technique within 1 minute.

1. Introduction

Magnetic core−shell nanostructures with porous shell hold a great promise for many applications, such as catalysis, separation, drug delivery, and sensing. The main advantage of using these structures is the facile separation from the reaction mixture through the use of an external magnet, which eliminates the necessity for cumbersome filtration and centrifugation procedures.[1] In addition, magnetically induced heating has been demonstrated to initiate chemical catalysis on demand.[2,3] In this respect, significant progress has been made in controlling the growth of porous shell on magnetic cores, particularly the mesoporous silica.[4,5] In contrast, the development of magnetic core with microporous shell, such as zeolite, remains a largely unexplored field. Zeolites, a series of microporous crystalline aluminosilicates, are widely applied in the fields of adsorption and catalysis,[6] and combined with magnetic nanoparticles appears to be a very promising prospect. For example, core@shell structures consisting of magnetite cores and zeolite silicalite-1 shells have been synthesized by Deng et al.[7] Due the high affinity for trypsin and excellent microwave-absorption ability of the magnetite cores, the author demonstrated that the core@shell structure is highly efficient for digestion of proteins. Magnetic zeolite γ-Fe_2O_3/TS-1 with core@shell structure has been prepared successfully and used as catalyst in photocatalytic degradation of phenol or 4-chlorophenol and thiophene oxidation.[8] A more detailed description of each magnetic zeolite composite type and their application is presented in the recent review.[9]

To date, three different synthesis methods have been used to synthesize core-zeolite shell structures; (i) seeded growth; (ii) *direct synthesis* and (iii) physical coating. [10] Cheng et al., prepared magnetic zeolite γ-Fe_2O_3/TS-1 with core-shell structure by using seeded growth method, and tested this nanostructure in the photocatalytic degradation of organic contaminants. It is important to emphasize that achieving a core-shell material with a shell thickness below

100 nm is still a challenge by using seeded growth approach, since the minimum shell thickness is limited to the size of the zeolite seeds (40–50 nm).[10] Such a drawback can be overcome using *in situ* method, wherein a coating process is favored by the simultaneous nucleation, adsorption, and growth of seeds on the surface of the core particles, all performed in a one-pot synthesis. Using *in situ* method, some authors have reported the use of these magnetic zeolites in the removal of different contaminants. For example, García-Aguilar et al., [11] prepared ferrite core with a well-defined shell of zeolite ZSM-5 by submitting a suspension of TiO_2-coated nickel ferrite nanoparticles to hydrothermal treatment in an aqueous precursor solution. Yu et al.,[12] used magnetic particles impregnated with zeolite A to remove ammonium from water, whereas Liu et al., [13] added magnetite particles to a zeolite A precursor solution in order to produce magnetic zeolites for posteriorly application to remove heavy metal ions from aqueous solutions. Despite that the previous studies have demonstrated the formation zeolite shell on magnetic particles, the competition between nucleation centers in the bulk gel and on the surface of the core particle resulting in abundant formation core-free zeolite particles has been also reported.[10] An alternative, and more practical approach is the physical coating where the microsized-core particles are coated by zeolite crystals using a binder.[14] This approach allows circumventing some of the main disadvantages of the previously mentioned techniques, including core dissolution and core-free zeolite formation. Nonetheless, the use of binder can decrease the concentration of active sites and their accessibility. Additionally, this technique is mainly applicable to recover microsized particles as a core.[10] While recent works on core-shell nanostructures are becoming increasingly in quantitative and insightful, synthesis techniques to prepare core-zeolitic shell nanostructures (< 100 nm) with discrete, uniform, and finely tunable shell thickness without the generation of core-free zeolite particles are still challenging.

Herein, we present a procedure to obtain magnetic γ-Fe_2O_3@$mSiO_2$ core-shell nanoparticles containing ultra-small domains of silicalite-1 (γ-Fe_2O_3@$mSiO_2$/Silicalite-1). It was found that a mixture comprising Fe_3O_4@$mSiO_2$ nanostructures and TPAOH as an OSDA under hydrothermal conditions enables a reorganization of amorphous TPA^+–silicate composites in the shell and further formation of ultra-small domains containing the secondary building units (SBU) of silicalite-1. In an effort to elucidate the formation of intermediates during the recrystallization of $mSiO_2$ into silicalite-1 zeolite, the structural, microstructural, and textural evolution of the products were characterized by X-ray diffraction (XRD), Raman spectroscopy, Fourier-transform infrared spectroscopy (FTIR), scanning electron microscope (SEM) with Energy dispersive X-ray (EDS), Transmission electron micrograph (TEM) and nitrogen physisorption. We also demonstrated that the γ-Fe_2O_3@$mSiO_2$/Silicalite-1 products show

promising functional properties such as superparamagnetism confirmed by the superconducting quantum interference device (SQUID) magnetometer measurements, and adsorption capacity for removing aniline from aqueous solution. These findings provide more options and insight into the prospective synthesis of nanosized core-shell structures containing zeolitic shell.

2. Results and discussion

2.1. Structural and textural characteristic of calcined samples

The main text of the article should appear here with headings as appropriate. The recrystallization of amorphous silica nanoparticles into silicalite-1 using tetrapropylammonium (TPA^+ cations as structure directing agent) in the presence of limited amounts of water has been previously reported.[15] We have used similar approach to recrystallize the $mSiO_2$ shell initially growth on the Fe_3O_4 nanoparticles into Silicalite-1. Figure 1a shows powder XRD patterns of the calcined products collected after hydrothermal treatment for different periods of time. No new Bragg reflections have been observed for the products prepared up to 12 h of hydrothermal treatment, and the solid product shows mainly a broad band at 20−25° (2θ), characteristic of amorphous silica. Typical Bragg diffraction peaks corresponding to the MFI framework structure started to appear in the XRD patterns of the sample Fe@Si-24, and the intensities of XRD peaks sharply increased for the sample Fe@Si-24. These peaks corresponding to the crystallographic planes of silicalite-1.[16] The XRD pattern of the sample hydrothermally treated up to 24 h also shows an additional peak at around 35.34° (2θ) as indicated by an arrow in Figure 1. This peak can be observed in the as-prepared products (Figure S4). The XRD pattern of precursor magnetic core (Figure S5) contains a peak that can be indexed to the (311) plane of the cubic structure of magnetite (JCPDS card No. 79-0416). Similar peak is observed for the as-prepared and calcined Fe_3O_4@$mSiO_2$ nanostructured samples (Figure S5). Noteworthy, magnetite and maghemite (γ-Fe_2O_3) have inverse-spinel structure with similar lattice spacing, and distinguishing between these two phases with diffraction is difficult for nanoparticles smaller than 20 nm.[17] Therefore, we further investigated the structure of the calcined product by Raman spectroscopy (Figure 1b), which allows distinguishing between different iron oxide compounds based on characteristic vibrational modes.[18] Three broad bands at 710, 483 and 350 cm^{-1}, which are assigned to A_{1g}, E_g and T_g, phonon modes of maghemite, respectively,[19] are observed for the series of samples obtained up to 24 of HT. Therefore, the Raman data indicate the presence of γ-Fe_2O_3 phase in the calcined samples and support that the diffraction peak observed at 35.34° 2θ in the XRD patterns correspond to the (311) plane of the γ-Fe_2O_3 phase (JCPDS card No. 39-1346). These observations are in a good agreement with the phase transition of Fe_3O_4 occuring under thermal treatment. The importance of the SiO_2 shell to hinder

the phase transformation of γ-Fe_2O_3 to hematite (α-Fe_2O_3) as a non-magnetic phase, during the calcination was shown.[20] Raman spectra also contain the characteristic bands of silicalite-1 at 825, 470, 373 and 292 cm^{-1},[21] emerging for the sample Fe@Si-24 and consequently increases in the intensity for the sample Fe@Si-48. This result indicates that the crystallinity of silicalite-1 increased with increasing the hydrothermal treatment, which is in a good agreement with the XRD data.

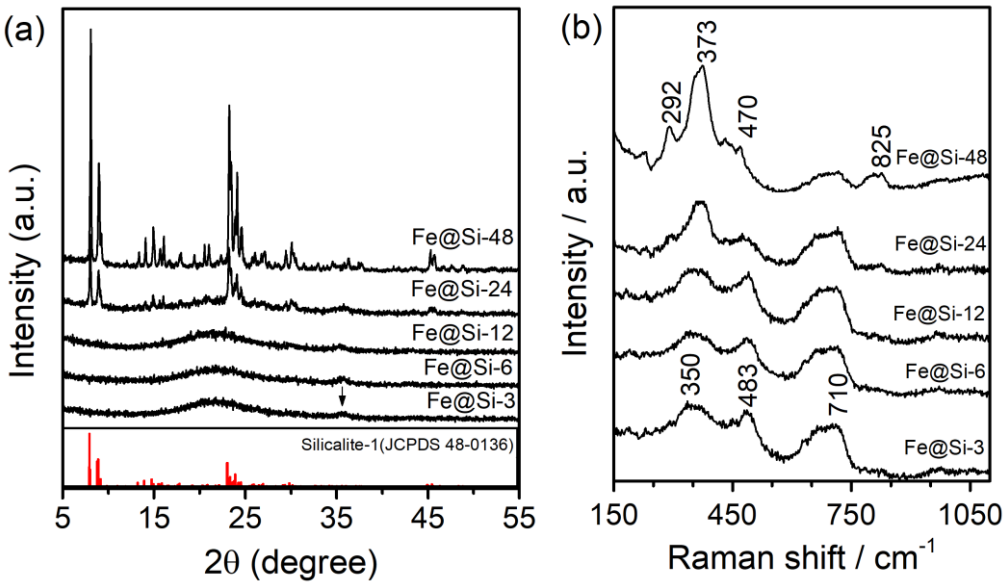

Figure 1. (a) XRD patterns and (b) Raman spectra of calcined samples after hydrothermal treatment for different periods of time (3 - 48 h).

Structural evolution of calcined products was further investigated by FTIR spectroscopy (Figure 2a). Compared to FTIR spectrum of precursor Fe@Si (Figure S6), the FTIR bands at 474, 802, and 1100 − 1300 cm^{-1} observed in the sample Fe@Si-3 can be assigned to the bending mode of Si−O, and symmetric stretch and asymmetric stretch of Si−O−Si, respectively.[22] A weak broad band at 592 cm^{-1} appears in the sample Fe@Si-6, which is assigned to the asymmetric stretching mode of the five-member rings (5MR) for MFI structure.[23] Noteworthy, this region overlaps with the bands at 636 and 577 cm^{-1} (Figure S6), assigned to the Fe–O stretching vibration of γ-Fe_2O_3 phase.[18] Therefore, a possible role of these bands cannot be excluded. With further hydrothermal treatment (sample Fe@Si-12), the band at 592 cm^{-1} is shifted to ca. 570 cm^{-1}, suggesting that the 5MRs are become more rigid, i.e. a shrinkage of 5MRs takes place.[23] This band has been assigned to the presence ultra-small domains containing SBU of silicalite-1.[24] In addition, the bending mode of Si−O shifts to 470 cm^{-1}, indicating a gradual increase in periodic structures. The band of 5MRs shifts to ca. 554 cm^{-1}

and two bands at 1109 and 1235 cm^{-1} can be observed for the sample Fe@Si-24. The latter bands are assigned to the external Si−O asymmetric stretching band of silicalite-1 phase. With further prolonging the HT, the intensity of these absorption increased, which is indicating the long-range crystalline order and growth of silicalite-1 crystals.[23] Further *in situ* adsorption of isobutanol was carried out to identify the formation of short range crystalline order in the silicate structure containing 5MRs after short time of HT.[25] Figure 2b shows FTIR spectra of isobutanol adsorbed in the calcined samples, where the characteristic CH_3 and CH_2 stretching vibration bands between 3000 and 2800 cm^{-1} are evident. [26] For the Fe@Si sample, isobutanol is only adsorbed on silanol groups as indicated by the presence of a band at 3745 cm^{-1}. The intensity of this band decreases with increasing the time of hydrothermal treatment, and completely disappears for the sample Fe@Si-48. Furthermore, an increase in the intensity of the bands in the region 3000−2800 cm^{-1} is observed. Interestingly; a dramatic increase in the normalized peak area was observed for the samples Fe@Si-12 and Fe@Si-24 (Figure 2b, inset), indicating that most of the accessible micropores are formed simultaneously with the formation of ultra-small domains containing SBU of silicalite-1.

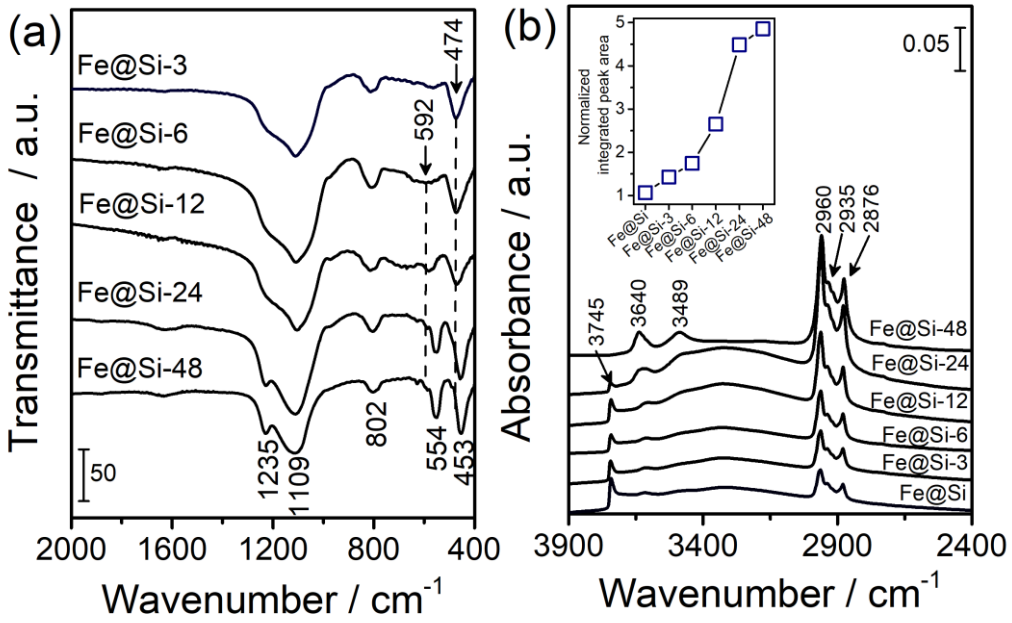

Figure 2. (a) FTIR spectra of samples prepared for different crystallization time (3-48 h) and (b) *in situ FTIR* spectra of isobutanol adsorbed at 35 °C on calcined samples prepared for different periods of time (3-48 h) in comparison to the initial Fe@Si sample. Inset; normalized peak area.

The textural properties of the calcined samples were studied by N_2 physisorption measurements (Figure 3). N_2 physisorption isotherms of samples Fe@Si-3 and Fe@Si-6 exhibited hysteresis loops corresponding to the mesopores with a pore size of 17 nm (Figure 3 inset). These samples show very similar N_2 physisorption isotherms, and a slight increase in the specific surface and mesopore volume (Table 1), when compared to the Fe@Si sample (Figure S7). As can be seen, the surface area of the samples increased with extending the HT treatment time from 6 h to 12 h. This result is attributed to the partial transformation of silica into zeolite and the generation of micropores in the silica shell (Table 1). The FTIR data are in a good agreement with this observation. The hysteresis loops due to mesopores and the sharp uptakes at low relative pressure, characteristic of micropores, simultaneously increased for the sample Fe@Si-24 (Figure 3). From the shape of the isotherm, we infer that a complex material containing micropores and mesopores are obtained after 12 and 24 h HT. We postulate that mesopores are further developed by partial dissolution of core-shell nanostructure as reflected in the broadening of the mesopore size distribution (Figure 3, inset). N_2 physisorption Type IV isotherm with a very small hysteresis loop for the sample Fe@Si-48 is measured, indicating the presence of micropores predominantly (Figure 2).

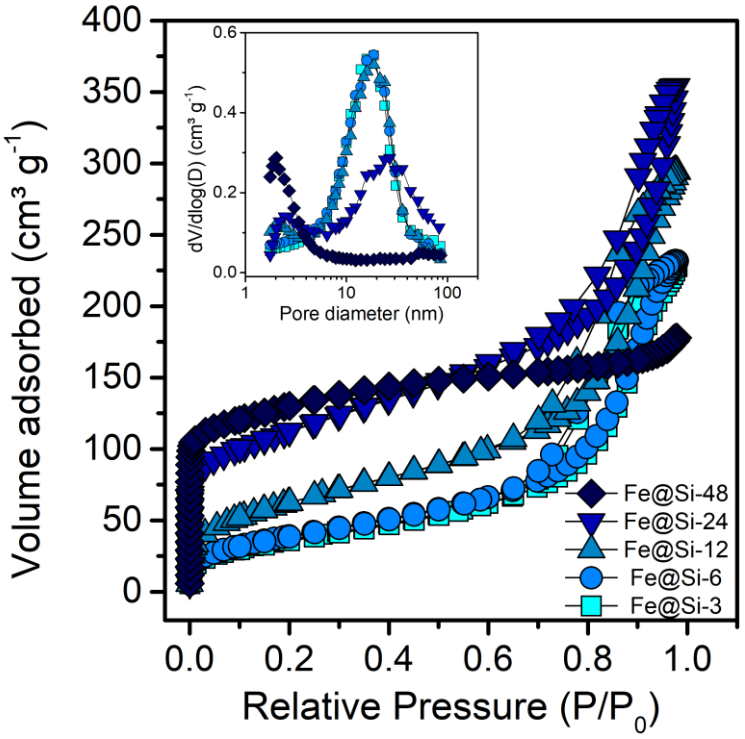

Figure 3. N_2 physisorption isotherms of calcined samples after hydrothermal treatment for different periods of time (3-48 h). *Inset:* pore size distribution curves.

Table 1. Textural properties of calcined samples after different time of HT treatment.

Sample	Surface area[a)] ($m^2\ g^{-1}$)	Micr. area[b)] ($m^2\ g^{-1}$)	V_{micro}[b)] ($cm^3\ g^{-1}$)	V_{total}[c)] ($cm^3\ g^{-1}$)
Fe@Si-3	132	-	0.00	0.34
Fe@Si-6	143	-	0.00	0.35
Fe@Si-12	226	30	0.03	0.43
Fe@Si-24	377	140	0.10	0.52
Fe@Si-48	478	295	0.13	0.29

[a)] Calculated by Brunauer–Emmett–Teller (BET) method from the adsorption data obtained at P/P_0 between 0.05 and 0.25.

[b)] Micropore area and volume determined by *t-plot* method.

[c)] Total pore volume determined via the single-point method.

3.2 Microstructural evolution of samples during the hydrothermal treatment.

The morphological change of the samples during the hydrothermal treatment was initially observed by SEM. Figure 4 shows selected SEM images of the microstructure of the precursor Fe_3O_4@mSiO_2 and as-synthesized products after 12h, 24h and 48 h HT treatment. The Fe_3O_4@mSiO_2 nanostructure (Figure 4a) consists of irregular aggregates formed by nanoparticles with spherical morphology (see TEM image in Figure S3a). No significant change in morphology was observed in the as-synthesized Fe@Si-12 samples (Figure 2a and Figure S8). Results from the XRD and Raman spectroscopy suggested the presence of silicalite-1 crystals domains for the sample Fe@Si-24 (Figure 1), and the SEM revealed the formation of crystals with a size of 100 - 200 nm (Figure 4c). The silicalite-1 crystal are embedded in the solid aggregates. However, large aggregates formed by micron-sized particles are also observed (Figure S8). According to the EDS elemental mapping, the Si-rich region is present in the as-synthesized sample Fe@Si-24, while Fe and Si are homogeneously distributed in the as-synthesized sample Fe@Si-12 (Figure S9). This result suggests a phase transition proceeds between 12 and 24 h HT treatment. Prolonged hydrothermal treatment to 48 h resulted in the formation of crystals with larger sizes of 250 − 460 nm with crystal-like facets, characteristic of silicalite-1 solely prepared in at 90 °C.

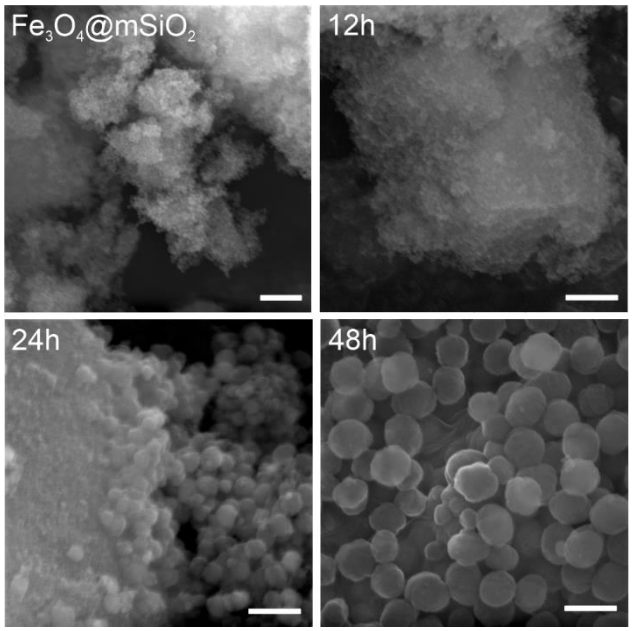

Figure 4. SEM images of the precursor Fe_3O_4@$mSiO_2$ nanostructure and of the as-synthesized samples after different HT times (scale bar = 500 nm).

Particle size of the samples along the hydrothermal treatment were investigated by DLS (Figure 5). The hydrodynamic diameter of the as-synthesized sample Fe@Si-3 with an average diameter of 91 nm is almost identical to the initial material prior hydrothermal treatment; the sample has nearly monodisperse particle size distribution (Figure S2c and S2d). A gradual shift to lower average sizes from 88 to 68 nm is observed for as-synthesized samples Fe@Si-6 and Fe@Si-12, respectively. Two distinctive peaks corresponding to particles a hydrodynamic diameter of 62 and 262 nm are observed for the as-synthesized sample Fe@Si-24. These results are consistent with the SEM observation (Figure 4) showing the formation of micron-sized particles after 24h HT. Finally, a monomodal size distribution of crystals with an average hydrodynamic size of 360 nm is observed for the as-synthesized sample Fe@Si-48. In addition to DLS size distributions presented as a function of scattering intensity (Figure 5a), the size distributions as a function of number of particles is also shown. A decrease in the average hydrodynamic diameter from 51 nm to 39 nm for the as-synthesized samples Fe@Si-3 and Fe@Si-24, respectively, is observed (Figure 5b). Note that a monodisperse particle size distribution curve is measured for the sample after 24 h HT which is different from the DLS intensity representation curve (Figure 5b). This is due to the fact that, in the DLS size distribution by numbers, the presence of a few large particles is masked by the large number of small particles. This result suggests that the product prepared after 24 h HT is mainly formed by nanoparticles with the average hydrodynamic size of 42 nm. For the as-synthesized sample Fe@Si-48,

particles with a diameter between 136 and 482 nm are formed (Figure 6b), which is in a good agreement with the particles size observed by SEM (Figure 4). DLS results show a decrease in the size of particles during the period 3 – 24h HT that clearly suggest a gradual dissociation of the silica shell. We monitored the rate of shell leaching of the Fe_3O_4@$mSiO_2$ particles under hydrothermal treatment for various times using DLS. The leaching rate is approximately 0.416 nm h^{-1} thus suggesting that the $mSiO_2$ shell has been leached completely after 37 h HT. The combination of microscopy and DLS analysis suggests that silicalite-1 crystals are formed after 24 h HT.

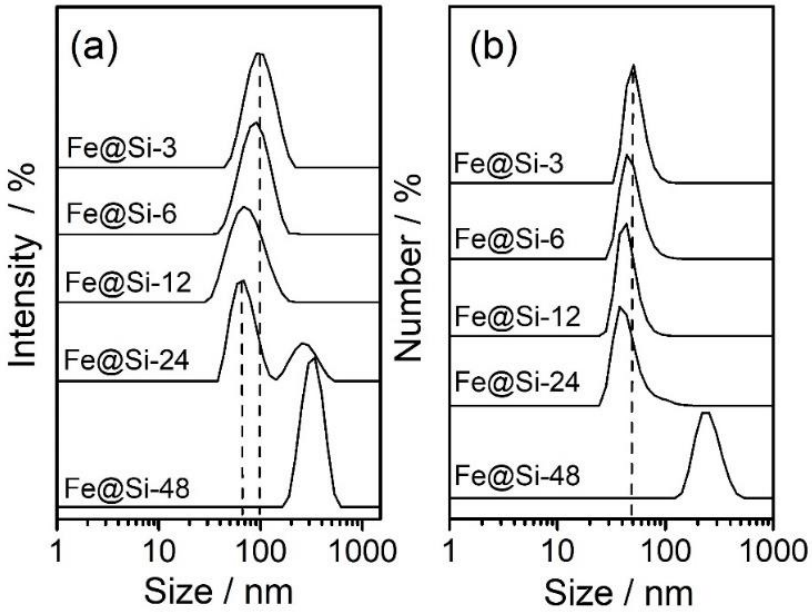

Figure 5 DLS particle size distribution curves expressed as a function of intensity (a) and number of particles (b) for as-synthesized samples prepared for different HT time (3-48 h).

To further observe the dissolution of the $mSiO_2$ shell and the microstructural evolution during the hydrothermal treatment, the as-synthesized samples were characterized by TEM (Figure 6). The core-shell nanostructure was well preserved after the hydrothermal treatment as shown in the TEM pictures. The as-synthesized samples Fe@Si-6, Fe@Si-12 and Fe@Si-24 contain monodisperse particles with mean diameters of 40.6, 36.4, and 32.4 nm, respectively. These results are consistent with the DLS analysis (Figure 5b). With increasing the HT time, not only the particles size decreases, but the silica shell surface became significantly rough. The rough surface would reflect on the larger surface area than the smooth one. Indeed, a slight increase in the specific surface area is observed for the samples Fe@Si-6 and Fe@Si-12 (Table1). In addition, the mesoporosity of the silica shell becomes higher as the HT increases, which is in a good agreement with the N_2 adsorption–desorption isotherms o the calcined products (Figure

3). Shell-free magnetic core is observed in the as-synthesized sample Fe@Si-24 thus confirming the dissolution of the $mSiO_2$ shell (Figure 6c, inset). As shown by HR-TEM (Figure 6b, d and f), the hydrothermal treatment leads to morphological changes as well. Interestingly, local periodic structure is clearly visible for the as-synthesized sample Fe@Si-12 (dotted circles in Figure 6d), while in the case of as-synthesized sample Fe@Si-24, ordered arrays of crystalline microporous framework can be observed (Figure 6f). Small crystalline domains have been observed within the amorphous phase during the initial stage of crystallization of zeolites.[27] These results strongly demonstrate that ultra-small domains containing SBU of silicalite-1 in the sample obtained for 12 h HT treatment are formed within the $mSiO_2$ shell, and further HT treatment improve the crystallinity of the particles, which is in accordance with FTIR analysis (Figure 2a). At 48 h HT treatment, the sample is composed by core-free silicalite-1 crystals and small aggregated nanoparticle (Figure S10). The crystalline structure of the small nanoparticles was confirmed by selected area electron diffraction (SAED) anaysis. The dot pattern of SAED corresponds to Fe_3O_4 (JCPDS card No. 19-0629) thus demonstrating that the hydrothermal treatment maintains the single crystal integrity of the core.

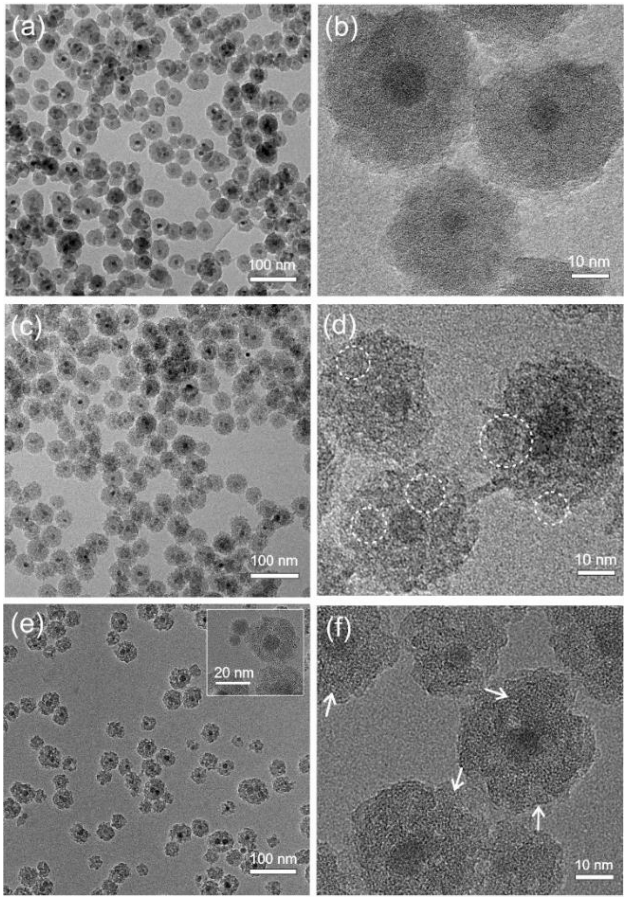

Figure 6 TEM images of as-synthesized samples (a,b) Fe@Si-6, (c,d) Fe@Si-12 and (e,f) Fe@Si-24. Arrows are pointing to different crystalline orientations of zeolite fringes in the $mSiO_2$ shell.

On the basis of our observations herein, we propose a scheme representing the formation of ultra-small domains of silicalite-1 in the shell of the composites during the hydrothermal treatment (Scheme 1). Initially, most TPA^+ species are present in the liquid phase, while a portion penetrate into the mesoporous silica shell (stage i). Dissolution of the $mSiO_2$ shell by etching occur during the hydrothermal treatment, yielding rough surface of the Fe_3O_4@$mSiO_2$ and release of Si species (stage ii). Upon further hydrothermal treatment, reorganization of the TPA^+−silicate species and formation of ultra-small crystalline domains containing the SBU of MFI type framework structure gradually proceeds (stage iii). After that, the TPA^+ −silicate shell grows via solid-state reorganization. As the $mSiO_2$ dissolution proceeds, the nucleation of silicalite-1 nanocrystals is driven by supersaturation of silicate species in the solution (stage iv), which is in line with previous reports.[28] Finally, larger silicalite-1 crystals are formed leading to a complete deletion of $mSiO_2$ shell and absence of core-shell nanostructure (stage v). It has been claimed recently that silicalite-1 crystal grows via a combination of classical and non-classical mechanisms by the addition of both silicate species and nanoparticle precursors, respectively.[29] We do not discard that ultra-small domain had been detached from the shell and then aggregates to silicalite-1 crystal at longer hydrothermal treatment times. The solid rearrangement of the amorphous SiO_2 shell into zeolite crystals may provide some guidance for further optimization of the synthesis process where other heteroatoms can be introduced in the structure of zeolite catalysts such as Al, B, Sn, etc.

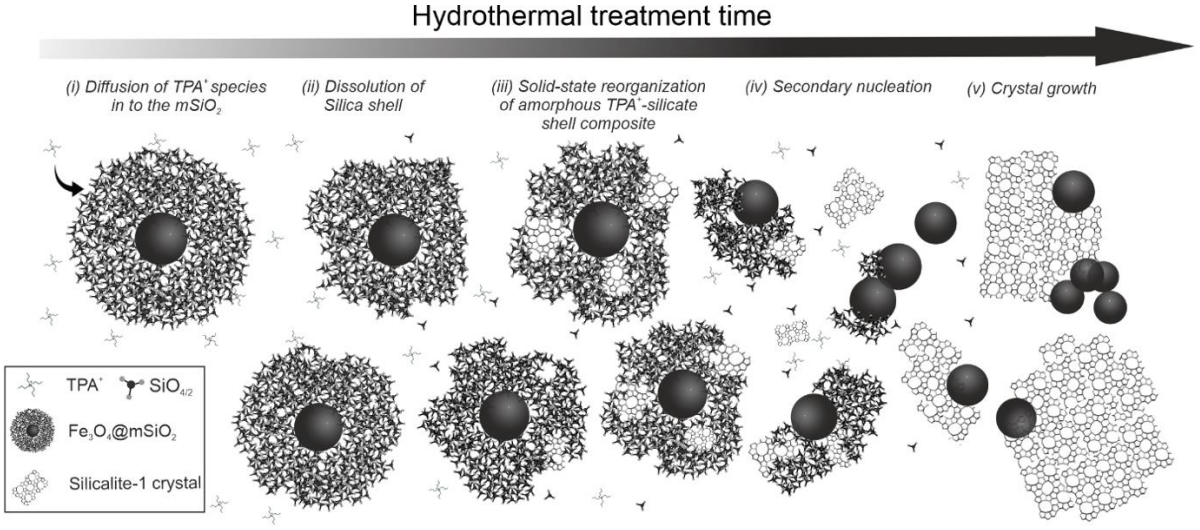

Scheme 1. Proposed scheme for the formation of γ-Fe_2O_3@$mSiO_2$/Silicalite-1 composite during hydrothermal treatment. Water molecules and hydroxyl anions are omitted for clarity.

3.3 Evaluation of adsorption performance

This type of nanostructure containing micro or mesopores can serve as potential adsorbent owing to the unique shape selectivity adsorption and easy separation by using external magnetic field. A preliminary adsorption study was performed using SiO_2/Silicalite-1 adsorbent for aniline removal from water.[30] The calcined samples were employed to adsorb aniline from an aqueous solution at pH 6.72 and room temperature. As shown in Figure 7a, the q_t increases sharply with an increasing the contact time, indicating a very rapid adsorption reaction between aniline and the solid surface. Indeed, more than 95% of the maximum adsorption capacity was achieved within the first 5 min. The adsorption capacity of sample Fe@Si-12 reaches 13.17 mg g^{-1}, while similar values were achieved for the samples Fe@Si Fe@Si-3 and Fe@Si-6 (5.01, 5.42 and 5.98 mg g^{-1}, respectively). Further, the samples Fe@Si-24 and Fe@Si-48 show increased adsorption capacity to 27.4 and 58.2 mg g^{-1}, respectively. As previously reported, the molecular size of aniline is 0.59 nm which is similar to the pores size of silicalite-1 (0.56 nm).[31] Zeolites showed distinct adsorption affinity to molecules with molecular size similar to their pores due the so-called close-fit theory.[32,33] It is suggested that, the increase of q_t is related to the presence of mesopores in sample Fe@Si-12 that facilitate the diffusion of aniline from the solution.

Further the magnetic properties of the samples were evaluated. The room-temperature magnetic characterization using a SQUID magnetometer indicates that the sample Fe@Si-12 possess a magnetization saturation value of 3.9 $emug^{-1}$ (Figure 7b). The coercivity and the remanence were found to be 11.6 Oe and 0.06 emu g^{-1}, respectively (Figure 8b, inset), which revealed that the superparamagnetic behavior of the magnetic nanoparticle core remains after the hydrothermal treatment and calcination steps. However, the saturation magnetization is considerably lower than the bear magnetic Fe_3O_4 nanoparticle core (43.6 emu g^{-1}), which is due to presence of non-magnetic shell.[22] Low saturation magnetization is also observed for the precursor Fe_3O_4@mSiO_2 (see Figure S11). Although saturation magnetization is relatively low, the product prepared after 12h could still be easily collected using an external magnetic field (Figure 7c).

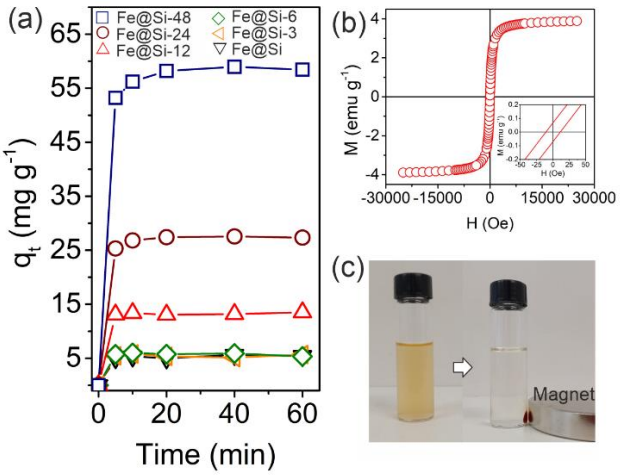

Figure 7. (a) Kinetic adsorption of aniline; (b) hysteresis loops measured at 300 K of the sample Fe@Si-12; and (c) a photo showing the magnetic separation by applying a magnetic field to the aniline solution in the presence of the sample Fe@Si-12 after 1 min (left).

3. Conclusion

In summary, we have reported an approach to synthesize nanosized (< 100 nm) and narrowly size-dispersed γ-Fe_2O_3@mSiO_2 nanoparticles containing ultra-small domains of silicalite-1 (γ-Fe_2O_3@mSiO_2/Silicalite-1). The strategy is based on the solid-state reorganization of the amorphous SiO_2 shell formed onto Fe_2O_3 into silicalite-1 using TPA^+ as an OSDA under hydrothermal conditions. The mechanism of formation of silicalite-1 shell during the hydrothermal treatment of the silica on γ-Fe_2O_3 is proposed. We also demonstrated that the calcined samples showed promising superparamagnetism, and the adsorption capacity towards aniline from aqueous solution is improved.

4. Experimental Section

Synthesis of Fe_3O_4@mSiO_2 nanostructures: All chemicals were of analytical grade and used without further purification. Fe_3O_4 nanoparticles (NPs) with a uniform diameter of 13.8 nm (Figure S1) were obtained by thermal decomposition.[34] In a typical preparation, 4 g of iron oleate complex were added to a solution containing 0.32 mL of oleic acid (Synth, P.A.) and 12.5 mL of 1-octadecene (Aldrich, 90 %). The resulting brown solution was stirred for 30 min and transferred to a three-necked round-bottom flask and heated to 320 °C for 60 min under a N_2 atmosphere. The solution was cool to room temperature, and the as-prepared solid was separated, washed several times with a mixture of hexane : acetone solution in a ratio of 1 : 4 (v/v), and finally dispersed in cyclohexane (5 mg mL^{-1}) for further use.

Fe_3O_4@mSiO_2 core-shell nanostructures with an average size of 50.7 nm and silica shell thickness close to 15.6 nm (see Figure S2 in the Supporting Information for additional details) were prepared by the reverse microemulsion method.[22] In a typical synthesis, 10 mL of Igepal CO-520 (Sigma-Aldrich) and 20 mL of the abovementioned Fe_3O_4 NPs dispersion were mixed with 160 mL of cyclohexane (Sigma-Aldrich, 99%) under ultrasonication for 10 min and then kept for 20 min under vigorous stirring. Subsequently, 2 mL of ammonium hydroxide (Synth, 25%−28%) was added dropwise under magnetic stirring. Finally, 4 mL of tetraethyl orthosilicate (Sigma-Aldrich, ≥99%) was added sequentially dropwise into the above suspension at a precisely controlled rate of 0.5 mL h^{-1} by using a Syringe Pump (KDS 100). Four times fractionated drop was adopted. After stirring the resulting mixture for 36 h, the Fe_3O_4@mSiO_2 nanostructures was precipitated using an excess of ethanol, washed several times with deionized water, and then stored in deionized water (5 mg mL^{-1}) for further use.

Recrystallization of mSiO_2 shell into Silicalite-1: The recrystallization of mSiO_2 shell into Silicalite-1 were performed under hydrothermal synthesis. In brief, 100 g the as-synthesized Fe_3O_4@mSiO_2 nanostructures were separated by centrifugation and then dispersed in TPAOH (1M), to which deionized water was added in order to prepare a well-dispersed suspension. The molar composition of this precursor slurry is 25SiO_2:4.5TPAOH:260H_2O (where SiO_2 precursor is mSiO_2 shell). Adequate amount of Fe_3O_4@mSiO_2 was used based on the ICP and TG results (Table S1). The resulting mixture was sonicated for 20 min and stirred for 30 min at room temperature. Then, the mixture was transferred to a 5 mL Teflon-lined autoclave and hydrothermally treated at 90 °C for different time (3, 6, 12, 24 and 48 h). After the prescribed synthesis time, the products were separated by centrifugation and subsequently washed with distilled water until the filtrate had an approximately neutral pH. The as-prepared products were dry at 80 °C overnight and calcined in air at 550 °C for 5 h. Calcined samples were named Fe@Si-h, where h is the time of hydrothermal treatment. The Fe_3O_4@mSiO_2 precursor was calcined at same condition and named Fe@Si.

Materials characterization: X-ray diffraction patterns were recorded using a PANalytical X'Pert Pro diffractometer equipped with a Cu Kα X-ray source (40 kV, 40 mA, λ = 1.5418 Å). Raman spectra were recorded on a confocal microprobe Raman system (Horiba Jobin Yvon Labram 300) at a fixed laser excitation of 532 nm. Dynamic light scattering (DLS) experiments were conducted on a Malvern Zetasizer Nano instrument equipped with a backscattering geometry (scattering angle of 173°, He−Ne laser with a wavelength of 632.8 nm). Fourier transform infrared (FTIR) spectra were recorded on a Nexus IR spectrophotometer using KBr. The morphology of the solid products was observed using a Tescan Mira I LMH scanning

electron microscope (SEM) under an accelerating voltage of 20 kV. Energy dispersive X-ray (EDX) analysis was performed using two Bruker XFLASH 6/30 EDX cameras. Transmission electron micrograph (TEM) images were obtained by a Philips FEI Tecnai G2 microscopy operating at 300 kV. Nitrogen physisorption analysis was carried out on a Micromeritics ASAP 2020 gas adsorption analyzer. Prior to analysis, the samples were degassed at 200 °C for 12 h. *In situ* FTIR adsorption of butanol were recorded with a Nicolet 6700. Inductively coupled plasma mass spectrometry (ICP-MS) measurements were recorded using a 7900 ICP-MS from Agilent Technologies. TGA was performed with a thermogravimetry analyzer (SETARAM SETSYS 1750 CS) under oxygen atmosphere from 25 to 800 °C at a heating rate of 5 °C min^{-1}. For the measurement of isobutanol adsorption IR spectra, the products were pressed into self-supported disks (2 cm^2 area, 20 mg cm^{-2}) and placed in an IR cell equipped with KBr windows. Spectra were recorded in the 400−4000 cm^{-1} range at 4 cm^{-1} with 128 scans. A homemade IR cell was used to evacuate the samples; then samples were heated up to 200 °C for 3 h under vacuum before the measurements. Precise amount of isobutanol (0.5 Torr) were introduced into the cell and kept in equilibrium for 10 min at 35 °C until their corresponding FTIR bands reached saturation. To allow the comparison of different products, the spectra were normalized to the samples' mass and plotted as absorbance per gram over the wavelength. Magnetization measurements were performed on a MPMS XL superconducting quantum interference device (SQUID) magnetometer at 25 °C.

Adsorption studies: The main text of the article should appear here with headings as appropriate. The adsorption of aniline was investigated using batch experiments at 25 °C as follows: 20 mg of adsorbents was dispersed into 20 mL of aqueous solutions with initial concentrations (C_0) equal to 200 mg g^{-1}. The mixture was sonicated for about 1 minute to ensure uniform dispersion and then vigorously stirred for different time. The adsorbent was separated by using a magnet. The supernatant solutions were subjected to UV−vis analysis (Varian Cary 4000 UV–vis spectrometer) for determining the equilibrium concentrations of aniline (C_t). The adsorption capacity, q_t (mg g^{-1}), was calculated as follows:

$$q_t = \frac{(C_0 - C_t)V}{M} \quad (1)$$

where C_t, V and M are the volume of the aqueous solution (L) and mass of the adsorbent (g), respectively (the calibration curve is presented in Figure S3).

Supporting Information

Supporting Information is available from the Wiley Online Library or from the author.

Acknowledgements

This work was funded by São Paulo Research Foundation (grant numbers 2020/02289-1 and 2018/25649-3) and the Centre for zeolites and nanoporous materials (CLEAR) supported by the Region of Normandy.

Conflict of Interest

The authors declare no conflict of interest.

Received: ((will be filled in by the editorial staff))
Revised: ((will be filled in by the editorial staff))
Published online: ((will be filled in by the editorial staff))

References

[1] L. M. Rossi, N. J. S. Costa, F. P. Silva, R. Wojcieszak, *Green Chemistry* **2014**, *16*, 2906.

[2] F. Mushtaq, X. Chen, H. Torlakcik, C. Steuer, M. Hoop, E. C. Siringil, X. Marti, G. Limburg, P. Stipp, B. J. Nelson, S. Pané, *Advanced Materials* **2019**, *31*, 1901378.

[3] W. Wang, G. Tuci, C. Duong-Viet, Y. Liu, A. Rossin, L. Luconi, J.-M. Nhut, L. Nguyen-Dinh, C. Pham-Huu, G. Giambastiani, *ACS Catal* **2019**, *9*, 7921.

[4] E. A. Schultz-Sikma, H. M. Joshi, Q. Ma, K. W. MacRenaris, A. L. Eckermann, V. P. Dravid, T. J. Meade, *Chemistry of Materials* **2011**, *23*, 2657.

[5] Z. Sun, X. Zhou, W. Luo, Q. Yue, Y. Zhang, X. Cheng, W. Li, B. Kong, Y. Deng, D. Zhao, *Nano Today* **2016**, *11*, 464.

[6] S. Mintova, M. Jaber, V. Valtchev, *Chem Soc Rev* **2015**, *44*, 7207.

[7] Y. Deng, C. Deng, D. Qi, C. Liu, J. Liu, X. Zhang, D. Zhao, *Advanced Materials* **2009**, *21*, 1377.

[8] Q. Lv, G. Li, H. Lu, W. Cai, H. Huang, C. Cheng, *Microporous and Mesoporous Materials* **2015**, *203*, 202.

[9] A. R. Loiola, R. A. Bessa, C. P. Oliveira, A. D. L. Freitas, S. A. Soares, F. Bohn, S. B. C. Pergher, *J Magn Magn Mater* **2022**, *560*, 169651.

[10] N. Masoumifard, R. Guillet-Nicolas, F. Kleitz, *Advanced Materials* **2018**, *30*, 1704439.

[11] J. García-Aguilar, J. Fernández-García, E. v. Rebrov, M. R. Lees, P. Gao, D. Cazorla-Amorós, Á. Berenguer-Murcia, *Chemical Communications* **2017**, *53*, 4262.

[12] M. Liu, B. Xi, L. Hou, S. Yu, *J Mater Chem A Mater* **2013**, *1*, 12617.

[13] H. Liu, S. Peng, L. Shu, T. Chen, T. Bao, R. L. Frost, *Chemosphere* **2013**, *91*, 1539.

[14] T. M. Lima, C. G. S. Lima, A. K. Rathi, M. B. Gawande, J. Tucek, E. A. Urquieta-González, R. Zbořil, M. W. Paixão, R. S. Varma, *Green Chemistry* **2016**, *18*, 5586.

[15] T.-L. Cui, X.-H. Li, L.-B. Lv, K.-X. Wang, J. Su, J.-S. Chen, *Chemical Communications* **2015**, *51*, 12563.

[16] J. Grand, S. N. Talapaneni, A. Vicente, C. Fernandez, E. Dib, H. A. Aleksandrov, G. N. Vayssilov, R. Retoux, P. Boullay, J.-P. Gilson, V. Valtchev, S. Mintova, *Nat Mater* **2017**, *16*, 1010.

[17] R. Hufschmid, H. Arami, R. M. Ferguson, M. Gonzales, E. Teeman, L. N. Brush, N. D. Browning, K. M. Krishnan, *Nanoscale* **2015**, *7*, 11142.

[18] X. Zhang, Y. Niu, X. Meng, Y. Li, J. Zhao, *CrystEngComm* **2013**, *15*, 8166.

[19] A. M. Jubb, H. C. Allen, *ACS Appl Mater Interfaces* **2010**, *2*, 2804.

[20] D. H. Piva, R. H. Piva, M. Picinini, A. D. Rodrigues, E. A. Urquieta-González, *Catal Commun* **2021**, *148*, 106182.

[21] F. Fan, Z. Feng, C. Li, *Chem Soc Rev* **2010**, *39*, 4794.

[22] H. L. Ding, Y. X. Zhang, S. Wang, J. M. Xu, S. C. Xu, G. H. Li, *Chemistry of Materials* **2012**, *24*, 4572.

[23] C. E. A. Kirschhock, R. Ravishankar, F. Verspeurt, P. J. Grobet, P. A. Jacobs, J. A. Martens, *J Phys Chem B* **1999**, *103*, 4965.

[24] D. Lesthaeghe, P. Vansteenkiste, T. Verstraelen, A. Ghysels, C. E. A. Kirschhock, J. A. Martens, V. van Speybroeck, M. Waroquier, *The Journal of Physical Chemistry C* **2008**, *112*, 9186.

[25] A. de Reviere, D. Gunst, M. K. Sabbe, M.-F. Reyniers, A. Verberckmoes, *Catal Sci Technol* **2021**, *11*, 2540.

[26] A. Farzaneh, M. Zhou, O. N. Antzutkin, Z. Bacsik, J. Hedlund, A. Holmgren, M. Grahn, *Langmuir* **2016**, *32*, 11789.

[27] M. Choi, K. Na, R. Ryoo, *Chemical Communications* **2009**, 2845.

[28] J. Grand, H. Awala, S. Mintova, *CrystEngComm* **2016**, *18*, 650.

[29] A. I. Lupulescu, J. D. Rimer, *Science (1979)* **2014**, *344*, 729.

[30] P. He, J. Ding, Z. Qin, L. Tang, K.-G. Haw, Y. Zhang, Q. Fang, S. Qiu, V. Valtchev, *Inorg Chem Front* **2020**, *7*, 2080.

[31] B. Smit, J. I. Siepmann, *Science (1979)* **1994**, *264*, 1118.

[32] X. Guo, H. Yun, M. Zhang, Q. Li, Q. Zhou, H. Shao, W. Hu, C. Li, S. Fan, *Ind Eng Chem Res* **2017**, *56*, 12024.

[33] D. J. de Ridder, J. Q. J. C. Verberk, S. G. J. Heijman, G. L. Amy, J. C. van Dijk, *Sep Purif Technol* **2012**, *89*, 71.

[34] J. Park, K. An, Y. Hwang, J.-G. Park, H.-J. Noh, J.-Y. Kim, J.-H. Park, N.-M. Hwang, T. Hyeon, *Nat Mater* **2004**, *3*, 891.

A facile method to prepare nanosized (< 100 nm) and narrowly size-dispersed magnetic core-shell containing ultra-small domains of silicalite-1 (γ-Fe_2O_3@mSiO_2/Silicalite-1) by the solid-state reorganization of the amorphous SiO_2 shell formed onto Fe_2O_3 into silicalite-1 using TPA^+ as an OSDA under hydrothermal condition. Additionally, adsorption capacity towards aniline from aqueous solution is improved due the presence of ultra-small domains of silicalite-1.

D. H. Piva*, R. H. Piva, S. Ghojavand, A. Pautrat, M. Debost, E. A. Urquieta-González, S. Mintova*

Synthesis of core-shell magnetic nanoparticles containing ultra-small domains of silicalite-1